J Supercond Nov Magn (2011) 24:2325–2329
DOI 10.1007/s10948-011-1193-6

ORIGINAL PAPER

Study of Microstructure and Magnetic Properties of SrM Hexaferrites with Neodymium Oxide

T.J. Pérez-Juache · I. Betancourt · S.A. Palomares-Sánchez · M. Mirabal García · J.A. Matutes-Aquino · A.L. Guerrero-Serrano

Received: 13 May 2011 / Accepted: 24 May 2011 / Published online: 18 June 2011

Abstract In this work, we report a systematic study on the microstructure and magnetic properties of isotropic M-type $SrNd_xFe_{12-x}O_{19}$ hexaferrites ($x = 0.0$, 0.1, 0.2, 0.3, 0.4, 0.5) obtained by conventional ceramic process. According to DRX analysis, a solid solution is formed for Nd contents up to $x = 0.1$, while a composite $Sr(NdFe)_{12}O_{19}/SrFeO_3$ microstructure results for $x > 0.1$. Interesting combinations of hard magnetic properties were obtained for the whole compositional series including increasing coercivity values (up to 329 kA/m for $x = 0.5$) with increasing Nd concentration, together with high Curie temperatures (around 731 K). Results are interpreted in terms of the Nd incorporation into the unit cell as well as within the frame of the nucleation controlled mechanism as the coercivity source for this kind of materials.

Keywords Hard magnetic materials · Sr-hexaferrites · Nucleation mechanism

T.J. Pérez-Juache (✉) · S.A. Palomares-Sánchez
Facultad de Ciencias, Universidad Autónoma de San Luis Potosí, Av. Salvador Nava Martínez S/N Zona Universitaria, San Luis Potosí, SLP, CP 78294, Mexico
e-mail: tepj2010@hotmail.com

I. Betancourt
Departamento de Materiales Metálicos y Cerámicos, Instituto de Investigaciones en Materiales, Universidad Nacional Autónoma de México, México D.F. 04510, México

M. Mirabal García
Instituto de Física, Universidad Autónoma de San Luis Potosí, Av. Dr. Nava S/N, Zona Universitaria, 78290, San Luis Potosí, SLP, México

J.A. Matutes-Aquino · A.L. Guerrero-Serrano
Centro de Investigación en Materiales Avanzados, Chihuahua, Chih., México

1 Introduction

Hexagonal ferrites are well known as permanent magnet materials since the 1950s when they were announced for the first time [1]. The large magnetocrystalline anisotropy associated with the magnetoplumbite structure characteristic of this kind of materials affords intrinsic coercivity values between 250 and 350 kA/m, well comparable with the low rare-earth content nanocomposite Nd–Fe–B hard magnets [2, 3]. Hard ferrites play a predominant role in the permanent magnet market because of their low price per unit of stored energy, which allows competitive large scale production, together with the wide availability of the raw materials, their excellent chemical stability and their high Curie temperature, usually located within the range 700–750 K [2, 4]. Although considered as low performance magnets because of their rather low maximum energy product (usually below 30 kJ/m^3), their use in a wide range of applications includes anisotropic segments for electric motors, anisotropic rings for loudspeakers and large anisotropic blocks for ore separation, among others. In particular, numerous trivalent substitutions for strontium M-type hexaferrites $SrAFe_{12}O_{19}$ have been reported in the specialized literature including A = Cr^{3+}, Al^{3+}, having variable effect on their magnetic performance, but replacements with rare earth ions such as Nd^{3+}, Gd^{3+} are less known [5, 6]. In this work, we report a systematic study on the effect of Nd^{3+} replacement for Fe^{3+} on both the microstructure and magnetic properties of isotropic M-type $SrNd_xFe_{12-x}O_{19}$ ($x = 0$–0.5) hexaferrites.

2 Experimental Techniques

The isotropic hexaferrite $SrNd_xFe_{12-x}O_{19}$ series with different substitution ratios x (= 0.0, 0.1, 0.2, 0.3, 0.4, 0.5)

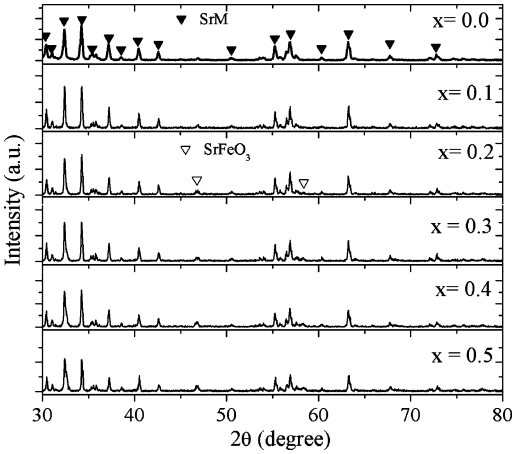

Fig. 1 XRD patterns for the $SrNd_xFe_{12-x}O_{19}$ series

were prepared by means of the conventional ceramic process. A mixture of α-Fe_2O_3, $SrCO_3$ and Nd_2O_3 powders in the required stoichiometric ratio was weighted and mixed for 2 hours at 90 rpm in a centrifugal planetary ball milling unit and then pre-sintered in air at 900°C for 1 hour; thereafter the fired powders were pressed into pellets, with polyvinyl alcohol (PVA) as a binder. The pellets were then sintered at 1200°C for 1 hour in air. Phase distribution, unit cell variation and grain size distribution were determined by means of XRD diffraction in a Bruker AXS D8 equipment. Scanning Electron Microscopy observations in a Leica Stereoscan 440 at 20 kV afforded verification of grain morphology and mean size. On the other hand, the magnetic properties at room temperature (saturation magnetization $\mu_0 M_s$, remanence $\mu_0 M_r$, intrinsic coercivity H_c and maximum energy product $(BH)_{\max}$) were determined by means of Vibrating Sample Magnetometry (VSM) in a LDJ 9600 equipment with $H_{\max} = 1250$ kA/m, while the Curie temperature was established by using Magnetic Thermogravimetric Analysis (MTGA) in a TA Instruments Thermobalance up to 850 K.

3 Results

X-ray diffractograms for the whole compositional $SrNd_xFe_{12-x}O_{19}$ series are shown in Fig. 1, for which the main peaks corresponding to the hexagonal M-type phase are present for all the patterns. In particular, at $x = 0.0$ and 0.1, no extra peaks related to secondary phases are observed in the diffractogram, indicating the formation of a solid solution for these Nd concentration levels. For increasing x (>0.2) the appearance of additional peaks at $2\theta = 46.7°$, 58.0° is consistent with the precipitation of the secondary $SrFeO_3$ phase according to the ICSD file #92335. The formation of this $SrFeO_3$ phase for the present hexaferrite series is due to the progressive excess of Sr^{2+} (relative to the original stoichiometry) caused by the substitution of Fe^{3+} by Nd^{3+} [7]. According to these XRD results, the incorporation of the Nd^{3+} into the unit cell seems to occur along the whole compositional interval, since no Nd-containing secondary phases were detected by XRD analysis.

SEM micrographs corresponding to $SrFe_{12}O_{19}$ and $SrNd_{0.4}Fe_{11.6}O_{19}$ hexaferrite samples are shown in Fig. 2. For the initial SrM sample (Fig. 2a), an isotropic distribution of hexagonal-shaped platelets is observed with an average size of 0.50 ± 0.14 μm, according to the grain size histogram on the right-hand side. In addition, the backscattered electron contrast is consistent with a single phase polycrystalline structure. On the other hand, for the $x = 0.4$ sample (Fig. 2b), the grain morphology tends to be refined and more rounded, with a mean size of 0.75 ± 0.19 μm according to the corresponding grain size histogram. In this case, it is also evident the presence of numerous minute grains (<0.25 μm) of different composition (according to the backscattered electron contrast), relative to the main constituent grains.

On the other hand, room temperature magnetic properties for the hexaferrite series $SrNd_xFe_{12-x}O_{19}$ ($x = 0$–0.5) as a function of the Nd content x are shown in Fig. 3. Both $\mu_0 M_s$ and $\mu_0 M_r$ (Fig. 3a) show a maximum at $x = 0.1$ followed by a progressive decrease, with the $(BH)_{\max}$ product (Fig. 3b) having a similar behavior. On the other hand, H_c exhibits a monotonous increase from 259 to 329 kA/m with increasing Nd concentration x (Fig. 3c). The Curie temperature also shows a shallow dependence on increasing Nd content, characterized by an initial decrease at $x = 0.1$, followed by slight variations for x beyond 0.1, as it is evidenced in Fig. 3d.

4 Discussion

The Nd incorporation into the crystal structure is supported by the Curie temperature variations recorded by MTGA experiments, which suggest an incipient weakening of the exchange interactions with increasing Nd concentration. In addition, the Nd^{3+} substitution into the hexagonal structure is expected to occur due to the accomplishment of the rule of charge conservation [2]. The marked reduction of $\mu_0 M_s$ and $\mu_0 M_r$ beyond $x = 0.1$ results from of the precipitation of the secondary Fe-containing phase $SrFeO_3$, whose antiferromagnetic ordering occurs at $T_N = 130$ K [8, 9]. The increasing volume fraction of this paramagnetic phase causes an increasing dilution effect of $\mu_0 M_s$. Complementarily, the tendency observed for the $(BH)_{\max}$ with the Nd content follows the $\mu_0 M_r$ behavior since the condition $\mu_0 H_c > 0.5 \mu_0 M_r$ is fulfilled [10]. In addition, all the samples manifest a noticeable remanence-enhancement effect as indicated by the M_r/M_s ratio which resulted in higher than the $0.5 M_s$ limit expected for uniaxial, non-interacting particles [11]. This effect can be associated with the exchange interaction coupling among surface magnetic moments on adjacent grains.

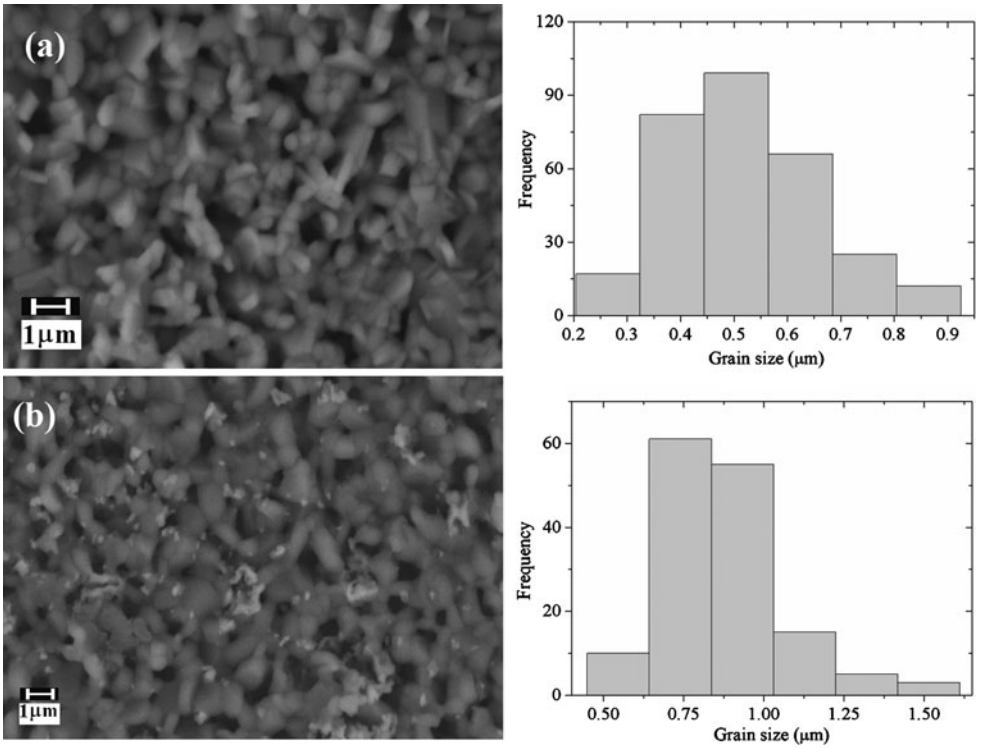

Fig. 2 SEM micrographs and grain size distribution for (**a**) $SrFe_{12}O_{19}$ and (**b**) $SrNd_{0.4}Fe_{11.6}O_{19}$ hexaferrites samples

This exchange coupling can be monitored by means of the Wohlfarth relation, which involves the following experimental parameters: the saturation remanence m_{sr} (obtained after removal of the magnetizing field in a positively saturated sample), the remanence $m_d\ (H)$ (after application and removal of a negative field $-H$ from m_{sr}) and the remanence $m_r\ (H)$ (after application and removal of a positive field H in an initially demagnetized sample) according to [11]:

$$m_d(H) = m_{sr} - 2m_r(H), \tag{1}$$

for which the plot $\delta M = m_d/m_{sr} - (1 - 2m_r/m_{sr})$ as a function of H, known as a Henkel plot, provides a useful way of representing the Wohlfarth relation. The positive part of δM is usually ascribed to the predominance of exchange interaction between neighboring grains, whilst the negative part of the curve represents the prevalence of the magnetostatic interaction [12–14]. The Henkel plots $\delta M(H)$ corresponding to the whole compositional series are displayed in Fig. 4. These curves are consistent with a magnetically coupled grained microstructure manifesting a dominant exchange interaction associated with the positive part of the δM curve up to a field of $H = 400$ kA/m, followed by the magnetostatic-type interaction at higher applied fields.

On the other hand, the progressive coercivity enhancement with increasing Nd content can be analyzed within the frame of the nucleation-controlled coercivity mechanism of coupled grains, for which H_c can be expressed as follows [10]:

$$H_c = H_N^{\min}\alpha_K - N_{\text{eff}}M_s \tag{2}$$

where $H_N^{\min}$ denotes the minimum nucleation field, and α_K and N_{eff} represent the effect of magnetic coupling among grains and the contribution of demagnetizing stray fields at sharp corners and edges of polyhedral grains, respectively. These parameters are thus intimately associated with the microstructure, making a significant contribution to the value of H_c. Additionally, the minimum nucleation field can be determined as follows:

$$H_N^{\min} = \frac{2K_1}{\mu_0 M_s}\alpha_\Psi^{\min}, \tag{3}$$

where $\alpha_\Psi^{\min}$ is also a microstructure parameter associated with the deleterious effect of misaligned grains on the ideal coercive field $H_c = H_N^{\min}$. For the condition of minimum nucleation field, $\alpha_\Psi^{\min} = 0.50$ [10]. For the calculation of $H_N^{\min}$, the parameters K_1, $\mu_0 M_s$ were determined by means of the law of approach to saturation for uniaxial crystals, which enables the fitting of the high-field part of the M–H curves according to [10]:

$$\mu_0 M(H) = \mu_0 M_s - \frac{4K_1^2}{15\mu_0 M_s}\frac{1}{H^2}. \tag{4}$$

The K_1, $\mu_0 M_s$ dependence on the Nd concentration x for the whole compositional series is exhibited in Fig. 5, for which a decreasing trend is manifested with increasing x.

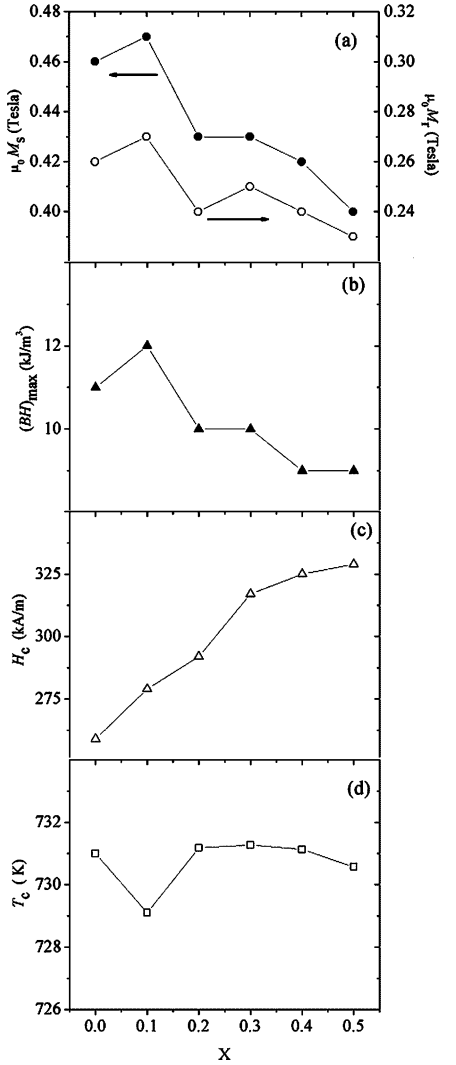

Fig. 3 Magnetic properties as a function of Nd content x for the hexaferrite series $SrNd_xFe_{12-x}$

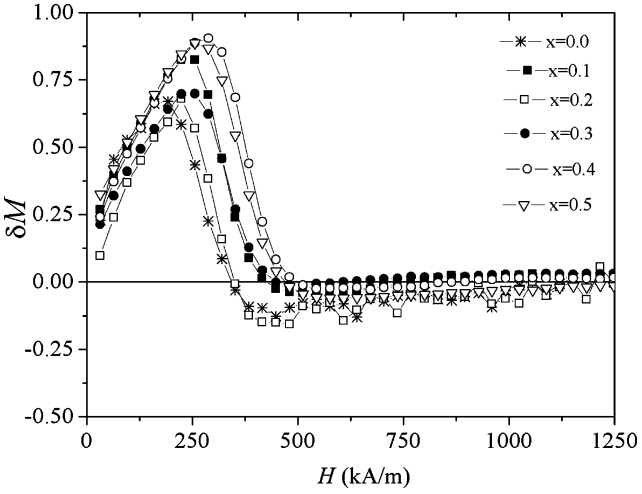

Fig. 4 Henkel plots $\square M(H)$ corresponding to the whole compositional series O_{19} (*solid lines* are only a guide for the eye)

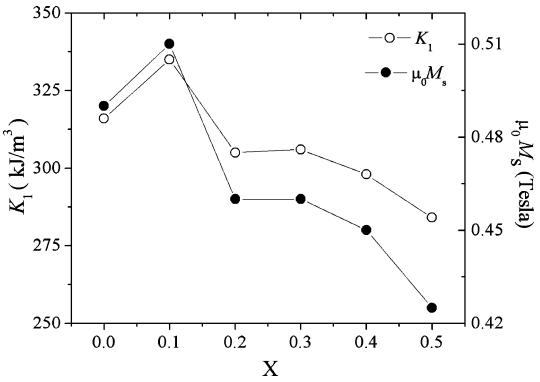

Fig. 5 The anisotropy constant K_1 and the saturation magnetization $\square M_s$, determined from the law of approach to saturation, Equation (4), as a function of the Nd concentration x for the hexaferrite series $SrNd_xFe_{12-x}O_{19}$ (*solid lines* are only a guide for the eye)

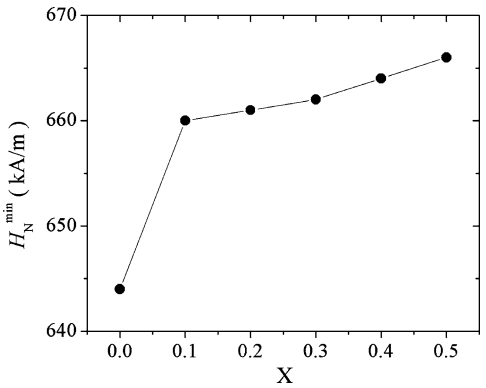

Fig. 6 The minimum nucleation field H_N^{min} as a function of the Nd content x for the hexaferrite series $SrNd_xFe_{12-x}O_{19}$ (*solid line* is only a guide for the eye)

The minimum nucleation field H_N^{min} for the whole composition interval is illustrated in Fig. 6 having a monotonous increase with Nd content. Therefore, the improving H_c observed across the Nd variation can be attributed to an enhancing effect on the minimum nucleation field as a result, on one hand, of the rapid decrease of μM_s values with x (Fig. 4) and, on the other hand, of microstructure effects provoked by the precipitation of secondary phases for $x > 0.1$, which affords reducing N_{eff} values with increasing x as a consequence of the formation of hard magnetic grains of more regular shape and size promoted by such additional phases.

5 Conclusions

Nd substituted SrM hexaferrites were synthesized by conventional ceramic method. Interesting combinations of hard magnetic properties were observed across the compositional series, with coercivity values well above 300 kA/m and high Curie temperatures around 731 K, rendering these materials

as suitable candidates for medium-performance, anisotropic, low-cost permanent magnets.

Acknowledgement T.J. Perez-Juache is grateful for the scholarship granted by CONACYT, Mexico, and the program for students mobility ECOES. Special thanks are due to L.E.G. Gabriel L. Rocha, M. en C. Raúl Ortega Zempoalteca and Dr. Lilia Narváez for their valuable technical assistance during the materials preparation and characterization.

References

1. Kojima, H.: In: Wohlfarth, E.P. (ed.) Ferromagnetic Materials, vol. 3, pp. 305–391. North-Holland, Amsterdam (1982)
2. Buschow, K.H.J.: Magnetism and processing of permanent magnets materials. In: Buschow, K.H.J. (ed.) Handbook of Magnetic Materials, vol. 10. Elsevier, Amsterdam (1997)
3. Betancourt, I., Davies, H.A.: J. Eng. Mater. Technol. **1**, 53 (2009)
4. Skomski, R., Coey, J.M.D.: Permanent Magnetism. Taylor & Francis, New York (1999)
5. Lechevallier, L., Le Breton, J.M., Morel, A., Tenaud, P.: J. Phys., Condens. Matter **20**, 175203 (2008) (9 pp)
6. Nga, T.T.V., Duong, N.P., Hien, T.D.: J. Alloys Compd. **475**, 55–59 (2009)
7. Wang, J.F., Ponton, C.B., Harris, I.R.: J. Magn. Magn. Mater. **298**, 122–131 (2006)
8. Jaya, S. Mathi, Jagadish, R., Rao, R.S., Asokamani, R.: Phys. Rev. B **43**, 13274 (1991)
9. Zhao, Y.M., Zhou, P.F.: J. Magn. Magn. Mater. **381**, 214 (2004)
10. Kronmuller, H., Manfred, F.: Micromagnetism and Microstructure of Ferromagnetic Solids. Cambridge University Press, Cambridge (2003)
11. Stoner, E.C., Wohlfarth, E.P.: Philos. Trans. R. Soc. **240**, 599 (1948)
12. Henkel, O.: Phys. Status Solidi **7**, 919 (1964)
13. Garcia-Otero, J., Porto, M., Rivas, J.: J. Appl. Phys. **87**, 73–76 (2000)
14. Liu, W., Liu, Y., Skomski, R., Sellmyer, D.J.: In: Liu, Y., Sellmyer, D.J., Shindo, D. (eds.) Handbook of Advanced Magnetic Materials, p. 226. Tsinghua University Press/Springer, New York/Beijing (2006)